Photoluminescence of $Cd_{1-x}Mn_xS$ ($x \leq 0.3$) Nanowires

Chan Woong Na, Doo Suk Han, Dae Sung Kim, Young Joo Kang, Jin Young Lee, and Jeunghee Park*

Department of Chemistry, Korea University, Jochiwon 339-700, Korea

Dong Keun Oh

Material Science Laboratory, Korea Basic Science Institute, Daejeon 305-333, Korea

Kil Suk Kim and Dongho Kim*

Center for Ultrafast Optical Characteristic Control and Department of Chemistry, Yonsei University, Seoul 120-749, Korea

Received: January 12, 2006; In Final Form: February 12, 2006

$Cd_{1-x}Mn_xS$ ($x = 0.1-0.3$) nanowires were synthesized by using the chemical vapor deposition method. They all consist of a single-crystalline wurtzite CdS structure with a [010] or [011] growth direction. The X-ray diffraction pattern reveals the contraction of the lattice constants due to the incorporation of Mn. The Mn^{2+} emission at ~2.15 eV, originating from the d−d ($^4T_1 \rightarrow {}^6A_1$) transition, appears below 50−80 K. Its decay time is in the range of 0.55−1 ms, showing a decrease with increasing Mn content. The Mn doping reduces significantly the decay time of band-edge emission from 590 ps to 20−30 ps. Upon applying magnetic field (up to 7 T), the Mn^{2+} emission is suppressed and donor−acceptor pair emission becomes dominant, suggesting the energy transfer from the band electrons to the Mn^{2+} ions.

1. Introduction

Diluted magnetic semiconductors (DMSs), in which host cations are randomly substituted by magnetic ions, have attracted considerable attention because of their potential use as the key materials in electronic devices.[1−4] For the integration into electronic devices, however, DMS materials will need to have low-dimensional structures, to make real use of the advantages offered by their spins. One of the important DMS nanosize materials, manganese (Mn)-doped cadmium sulfide (CdMnS) nanoparticles (or nanocrystals, quantum dots (QDs)), was synthesized with various methods.[5−15] Their optical properties as well as the magnetic moments of the incorporated Mn^{2+} ions have been extensively studied by a number of research groups. Yang et al. demonstrated bioimaging applications by making use of the Mn^{2+} emission and paramagnetism of CdMnS/ZnS core/shell QDs.[13c] Currently, a tremendous amount of research activity is underway on the synthesis and utilization of DMS 1-dimensional (1-D) nanostructures as well-defined building blocks for the fabrication of various nanoscale devices.[16] The syntheses of Mn (<10%)-doped CdS nanowires via hydrothermal reaction and chemical vapor deposition (CVD) methods were previously reported.[17,18] However, it is necessary to establish the method of controlling their Mn content in a wider range. Furthermore, detailed information needs to be obtained about the roles played by the doped Mn in their magnetooptical properties.

Herein, we report the successful synthesis of single-crystalline $Cd_{1-x}Mn_xS$ NWs, where x is in the range of 0−0.3, using the CVD method. The synthesis of nanowires doped with controlled Mn content opens up new opportunities for fundamental studies of physical phenomena in 1-D nanostructures. Therefore, we were able to measure the distinctive photoluminescence (PL) and magneto-PL properties of these $Cd_{1-x}Mn_xS$ DMS nanowires, and investigated intensively their remarkable excited-state dynamics following photon absorption. In particular, the emission properties of CdMnS NWs under applied magnetic field would be important in launching their promising role as building blocks of nanoscale magnetooptical devices.

2. Experimental Section

CdS (99.98%, Aldrich)/$MnCl_2$ (99.99%, Aldrich) powders were placed a few centimeters apart from an Au nanoparticle-deposited Si substrate, inside a quartz tube reactor. As the source evaporates at 850 °C for 1 h under argon flow, high-density Mn-doped CdS NWs deposit on the substrates at about 700 °C. The undoped CdS NWs were synthesized with use of only CdS powders under the same conditions. The Mn content was controlled by adjusting the temperature and position of the source. The products were analyzed by scanning electron microscopy (SEM, Hitachi S-4700), field-emission transmission electron microscopy (TEM, FEI TECNAI G^2 200 kV and JEOL JEM 2100F), high-voltage TEM (HVEM, JEOL JEM ARM 1300S, 1.25 MV), and energy-dispersive X-ray fluorescence spectroscopy (EDX). High-resolution X-ray diffraction (XRD) patterns were obtained by using the 8C2 beam line of the Pohang Light Source (PLS) with monochromatic radiation ($\lambda = 1.54520$ Å). The temperature-dependent steady-state photoluminescence (PL) measurements were carried out with use of an He−Cd laser ($\lambda = 325$ nm) as the excitation source. The laser power is below 1 MW/cm^2. The time-resolved PL spectrum was recorded with an ns-pulse Nd:YAG laser ($\lambda = 266$ or 355 nm, Coherent

* Address correspondence to these authors. E-mail: parkjh@korea.ac.kr and dongho@yonsei.ac.kr.

10.1021/jp060224p CCC: $33.50
Published on Web 03/09/2006

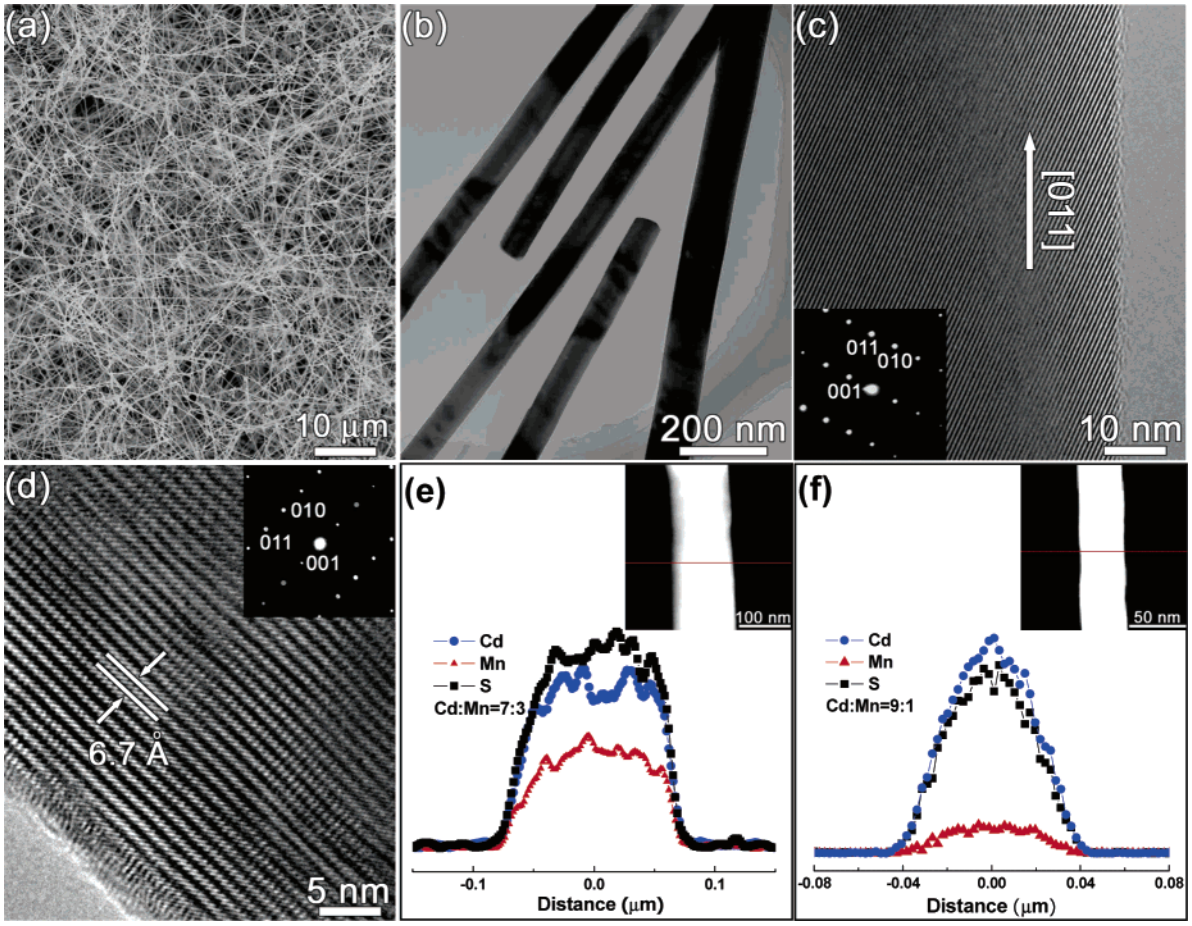

Figure 1. (a) SEM image showing the $Cd_{0.7}Mn_{0.3}S$ NWs grown on the substrate. (b) TEM image showing the general morphology of the $Cd_{0.7}Mn_{0.3}S$ NWs. Atomic-resolved image of the nanowires grown in the (c) [011] and (d) [010] growth directions. The SAED pattern reveals the single crystallinity with uniform growth direction (insets). The distance between the neighboring (001) planes is 6.7 Å. EDX line scanning of Cd, S, and Mn, for individual (e) $Cd_{0.7}Mn_{0.3}S$ NW and (f) $Cd_{0.9}Mn_{0.1}S$ NW.

Surelite). The time-correlated single-photon counting (TCSPC) system consisted of a self-mode-locked and cavity-dumped fs Ti-sapphire laser ($\lambda = 420$ nm) pumped by a continuous wave Nd:YAG laser (Coherent Verdi). The magneto-PL measurements were carried out under the magnetic field (up to 7 T) of a superconducting quantum interference device (SQUID, Quantum Design) magnetometer, using an He−Cd laser ($\lambda = 325$ nm).

3. Results and Discussion

As $CdS/MnCl_2$ powders evaporated, 1-D nanostructures deposit on Au nanoparticles-deposited Si substrate at about 700 °C. Figure 1a shows the SEM image of high-density wirelike nanostructures synthesized on a large area of substrate. Their length is about 20 μm. The TEM image reveals that they are all straight and have a smooth surface without any nanoparticle impurities (Figure 1b). Their average diameter is 80 nm. The HVEM images show highly crystalline nanowires grown in the [011] (Figure 1c) and [010] (Figure 1d) directions, without any amorphous outer layers or nanoparticles on the surface. In Figure 1d, the (001) fringes are separated by a distance of about 6.7 Å, which is close to that of wurtzite CdS crystal ($a = 4.14092$ Å and $c = 6.7198$ Å; JCPDS Card No. 41-1049). The selected-area ED (SAED) pattern shows a single-crystalline wurtzite structured CdS crystal (insets). The EDX line scanning identifies the Mn content ([Mn]/[Cd] + [Mn]) of the individual nanowires to be about 0.3, with a uniform distribution of the elements along the cross section (Figure 1e). The EDX analysis of many other nanowires indicates the average Mn content to be 0.3. We also synthesized high-purity single-crystalline undoped and Mn-doped CdS NWs with other Mn contents, viz. $x = 0.1$, 0.2, under the same conditions. All of the nanowires that we observed had either a [011] or a [010] growth direction. Figure 1f corresponds to an EDX line scanning for $Cd_{0.9}Mn_{0.1}S$ NW, showing uniform distribution of 10% Mn along the cross section.

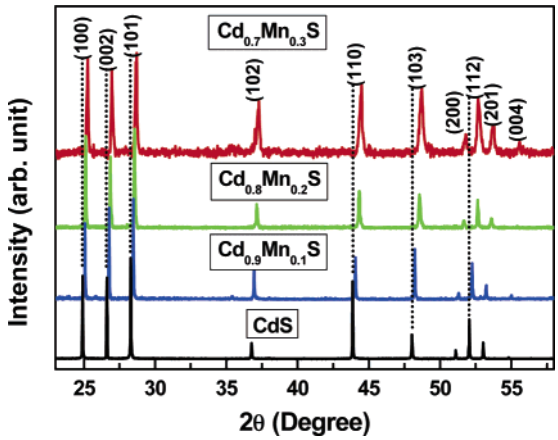

Figure 2. XRD pattern recorded for the CdS, $Cd_{0.9}Mn_{0.1}S$, $Cd_{0.8}Mn_{0.2}S$, and $Cd_{0.7}Mn_{0.3}S$ NWs, showing a significant higher angle shift due to the Mn doping.

The XRD pattern of the $Cd_{1-x}Mn_xS$ ($x = 0$, 0.1, 0.2, and 0.3) NWs confirms that their structure corresponds to that of highly crystalline wurtzite CdS crystals without formation of

TABLE 1: Reduction of the Lattice Constants and the Average Decay Time of Photoluminescence for $Cd_{1-x}Mn_xS$ Nanowires

	change of lattice constants (Å)		$^4T_1 \rightarrow {}^6A_1$ transition of Mn^{2+}		I_2-line	DAP at $H = 7$ T	
x	Δa (%)[a]	Δc (%)	λ (eV)	τ (ms)	λ (eV)	τ (ps)	λ (eV)
0	0[b]	0			2.547	590	
0.1	−0.0139 (−0.34)	−0.0198 (−0.30)	2.19	1	~2.6	31	2.478
0.2	−0.0409 (−0.99)	−0.0468 (−0.70)	2.16	0.7	~2.6	27	2.517
0.3	−0.0509 (−1.23)	−0.0818 (−1.22)	2.15	0.55	~2.6	22	~2.6

[a] The parentheses correspond to the percentage of lattice constant reduction. [b] The lattice constant of CdS nanowires is consistent with that of CdS crystal ($a = 4.14092$ Å and $c = 6.7198$ Å; JCPDS Card No. 41-1049).

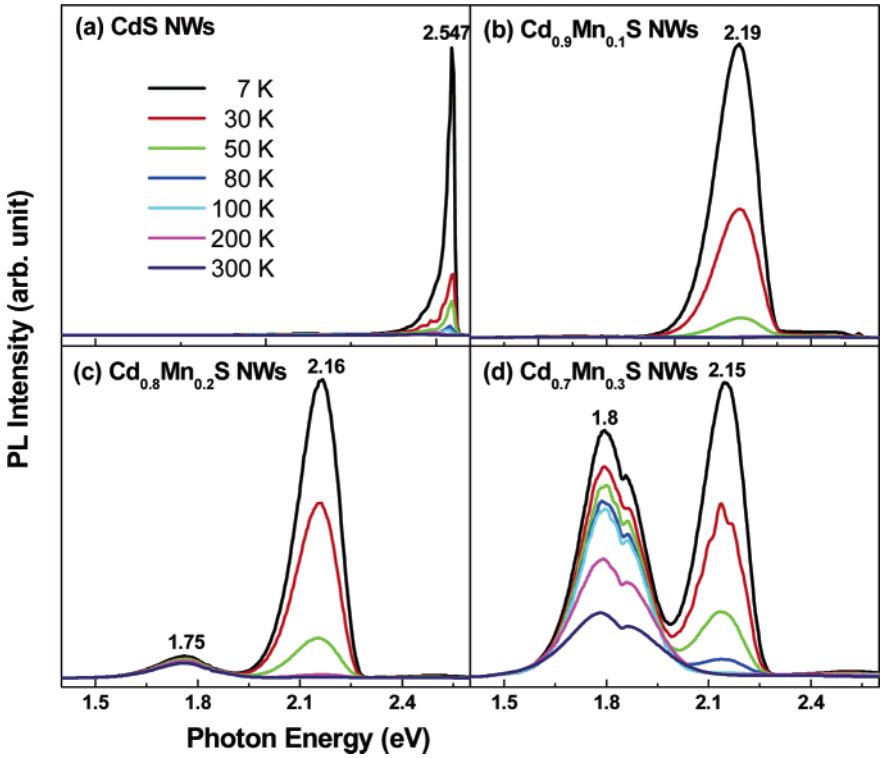

Figure 3. Temperature-dependent PL spectra of the (a) CdS, (b) $Cd_{0.9}Mn_{0.1}S$, (c) $Cd_{0.8}Mn_{0.2}S$, and (d) $Cd_{0.7}Mn_{0.3}S$ NWs. The excitation wavelength is 325 nm (3.815 eV) from the He−Cd laser.

other phases such as Cd or Mn oxides (Figure 2). The peak position of the undoped CdS NWs exactly matches that of wurtzite CdS crystal. As the Mn concentration increases, the peak position shifts significantly to a higher angle relative to that of the CdS NWs. The substitution of the Cd^{2+} ions ($r_{Cd^{2+}} = 0.92$ Å) with the smaller radius Mn^{2+} ions ($r_{Mn^{2+}} = 0.80$ Å) results in a reduction of the lattice constants of CdS. The reduction of lattice constants (a and c) due to the Mn doping has been estimated from the peak shift $\Delta(2\theta)$ of (100), (002), (200), and (004) peaks, as listed in Table 1. The lattice constants of the CdS unit cell decrease almost linearly with the Mn content, and reach up to 1.2% for $x = 0.3$. This contraction is consistent with that of the bulk, following Vegard's law.[19] The peak width increases with the Mn content, implying that the Mn incorporation deteriorates the crystallinity of CdS NWs.

Figure 3 shows the temperature-dependent steady-state PL spectrum of the undoped CdS and $Cd_{1-x}Mn_xS$ ($x = 0.1$, 0.2, and 0.3) NWs. The excitation wavelength is 325 nm (3.815 eV). The undoped CdS NWs exhibit a strong narrow peak at 2.547 eV (at 7 K), corresponding to the I_2 line that is responsible for the recombination of excitons bound to neutral donors (Figure 3a).[20] As the Mn is doped, the intensity of band-edge emission is drastically reduced, and the peak position is shifted to ~2.6 eV. Remarkably, the peak at around 2.15 eV, which originates from the d−d ($^4T_1 \rightarrow {}^6A_1$) transition of the tetrahedrally coordinated Mn^{2+} states, becomes dominant at low temperatures below 50−80 K (Figure 3b−d). The peak position shifts to a lower energy with increasing Mn content—2.19, 2.16, and 2.15 eV respectively for $x = 0.1$, 0.2, and 0.3, indicating that the Mn^{2+} concentration is sufficient to influence the crystal-field splitting between the $^4T_1$ and $^6A_1$ states. For $x = 0.2$ and 0.3, there is another band at ~1.8 eV nearby the Mn^{2+} emission band, persisting up to room temperature, and its intensity increases with the Mn content (Figure 3c,d). This red emission band was frequently observed in the case of both the nanocrystals and bulk.[12,21,22] If the tetrahedral crystal field is severely distorted or if there are sites with octahedral symmetry, due to the high Mn content, the crystal field is stronger and the states within the 3d shell are significantly affected. The Mn^{2+} ions present at such lattice sites show a different crystal-field splitting and, therefore, the emission bands are red-shifted. It is most important that the Mn^{2+} emission band originating from the $^4T_1 \rightarrow {}^6A_1$ transition shows a significant enhancement at low temperatures below 50−80 K for all three Mn contents. This result is similar to that of the film,[21] but distinctive from the strong Mn^{2+} emission of the nanoparticles/nanocrystals even at room temperature,[5−8] which needs further clarification. Nevertheless, the appearance of Mn^{2+} emission is strongly

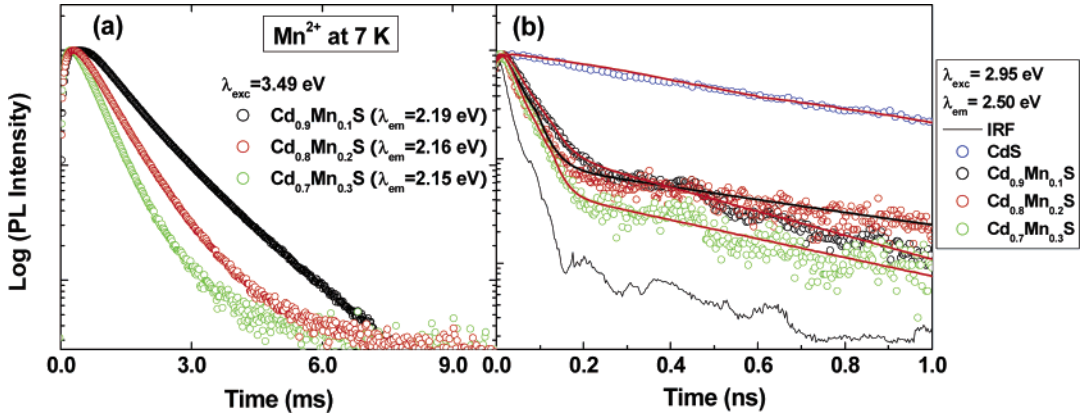

Figure 4. (a) Time-resolved PL spectrum of Mn^{2+} emission for the $Cd_{0.9}Mn_{0.1}S$, $Cd_{0.8}Mn_{0.2}S$, and $Cd_{0.7}Mn_{03}S$ NWs at 7 K. The excitation energy (λ_{exc}) is 3.49 eV, from the ns-pulse 355 nm Nd:YAG laser. (b) TCSPC data of the undoped CdS, $Cd_{0.9}Mn_{0.1}S$, $Cd_{0.8}Mn_{0.2}S$, and $Cd_{0.7}Mn_{0.3}S$ NWs at 2.5 eV. The excitation energy is 2.95 eV, from a frequency-doubled fs Ti-sapphire laser. The dotted line represents the instrumental response function (IRF). The data points (hollow circles) were fitted with biexponential decay function (red line) after data devolution, using IRF.

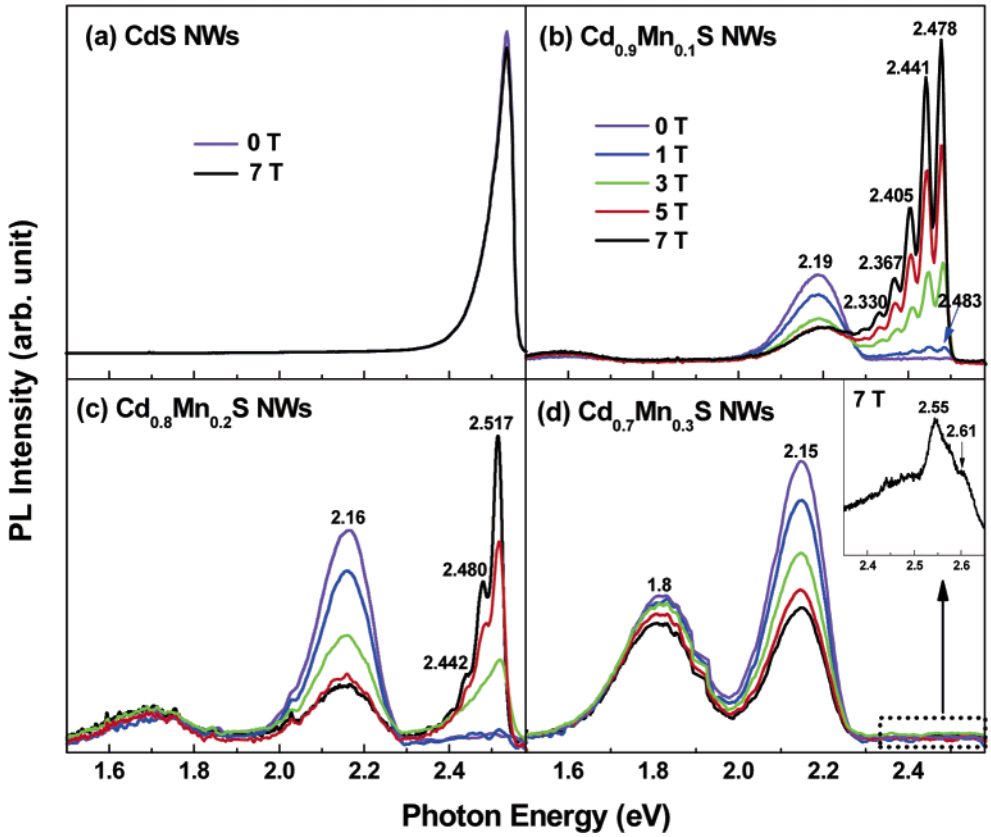

Figure 5. Magneto-PL spectrum of (a) CdS, (b) $Cd_{0.9}Mn_{0.1}S$, (c) $Cd_{0.8}Mn_{0.2}S$, and (d) $Cd_{0.7}Mn_{0.3}S$ NWs at 5 K, under $H = 0-7$ T. The excitation energy is 3.815 eV from the He−Cd laser. The inset in part d corresponds to a magnified scaled spectrum in the range 2.35−2.65 eV, under $H = 7$ T.

correlated with the efficient doping of Mn^{2+} ion into the tetrahedrally coordinated sites of the CdS crystal.

The time-resolved PL spectrum of the Mn^{2+} emission at 7 K, excited by 355 nm (3.49 eV), is displayed in Figure 4a. The fitting of decay parts with the biexponential function provides an average decay time of 1 ms for $x = 0.1$, 0.7 ms for $x = 0.2$, and 0.55 ms for $x = 0.3$, showing a decrease with increasing Mn content. These values remain nearly the same until 40 K, thereby providing the lifetime of the Mn^{2+} excited states. They are within the same time scale as that of the nanocrystals and bulk.[5b,11,21] For the faster decay rate of the band-edge emission, we employed the TCSPC system using the fs Ti-sapphire laser (2.95 eV). Figure 4b displays the room-temperature decay curve of the emission band at 2.5 eV. The data points of the decay part were fitted with the biexponential decay function after data devolution, using the instrumental response function (IRF). The average decay time of CdS NWs is 590 ps, which is somewhat shorter than that (~1 ns) of colloidal nanocrystals.[23,24] As the Mn is doped, the decay time is decreased significantly—31 ps for $x = 0.1$, 27 ps for $x = 0.2$, and 22 ps for $x = 0.3$, indicating that the Mn interaction would quench significantly to other shallow bound states. Table 1 summarizes the peak position and decay time of the I_2 line and Mn^{2+} emission, depending on the Mn content.

To provide more insight into the energy transfer process to produce the excited Mn^{2+} state, we measured magneto-PL of the undoped CdS and $Cd_{1-x}Mn_xS$ ($x = 0.1$, 0.2, 0.3) NWs at 5 K, by applying a magnetic field (H) in the range of 1−7 T, as

shown in Figure 5. The pure CdS NWs show no change of PL under the magnetic field up to 7 T (Figure 5a). As the magnetic field is increased to 7 T, the Mn^{2+} emission band of $Cd_{0.9}Mn_{0.1}S$ NWs is drastically suppressed, but a series of sharp emission peaks separated by ~0.038 eV, corresponding to the transverse optical (TO) phonon mode 305 cm^{-1},[25] becomes significant (Figure 5b). These peaks would be attributable to a zero phonon line and its phonon replicas of donor−acceptor pair (DAP) emission.[26] The appearance of such sharply separated DAP peaks reflects the highly crystalline nature of the present nanowires. In the case of the $Cd_{0.95}Mn_{0.05}S$ film, a strong increase of photoconductivity under an applied magnetic field was explained by the suppression of the Auger-type recombination process involving the excitation of Mn^{2+} ions.[27] The decreased Mn^{2+} emission intensity of the nanowires also would be due to the suppressed Auger-type recombination process, i.e., the energy transfer processes between band electrons and Mn^{2+} ions. This suppression effect arises from spin polarization of excess carriers and Mn^{2+} ions by applied magnetic fields. Therefore, the present magneto-PL result suggests that the excitation of Mn^{2+} involves the energy transfer from the band excitons. As the Mn content increases to $x = 0.2$, the sharpness and enhancement effect of DAP peaks is much reduced (Figure 5c). In the case of $Cd_{0.7}Mn_{0.3}S$ NWs, the intensity of DAP emission is very weak even at $H = 7$ T (Figure 5d). The inset corresponds to magnified scaled DAP peaks, showing no sharp phonon replicas. This decreased intensity of DAP emission could be related to the deteriorated CdS crystallinity by the Mn^{2+} incorporation. The red emission band at 1.8 eV is also suppressed by the magnetic field, providing evidence that its origin is also the coordinated Mn^{2+} ions.

As the Mn content is increased from $x = 0.1$ to 0.2, the zero phonon line of DAP emission at $H = 7$ T is shifted from 2.478 to 2.517 eV. In $Cd_{0.7}Mn_{0.3}S$ NWs, its position is approximately either 2.55 or 2.61 eV (inset of Figure 5d). This result suggests that the band gap (E_g) of $Cd_{1-x}Mn_xS$ NWs increases with increasing Mn content, which is consistent with that of the nanoparticles and bulk.[6,15,28,29] It is also consistent with the XRD result that the lattice constants decrease with the Mn doping. The corresponding band gap increase for the Mn content $x = 0.1-0.3$ could be estimated to be $\Delta E_g = \sim 100$ meV, which is nearly the same as that (~150 mV) of the bulk counterparts.[28,29] As the magnetic field increases from 1 to 7 T, the zero phonon line of DAP emission shifts from 2.483 to 2.478 eV for $Cd_{0.9}Mn_{0.1}S$ NWs. The spin splitting of the conduction and valence bands results in the decreased band gap, which is in agreement with the magnetic-field dependence of the absorption edge in wide band gap DMS.[27,30]

4. Conclusions

We synthesized undoped CdS and $Cd_{1-x}Mn_xS$ ($x = 0.1$, 0.2, and 0.3) NWs using the CVD method. They all consist of single-crystalline wurtzite structured CdS with a [010] or [011] growth direction. The XRD pattern shows the contraction of the lattice constants, confirming the incorporation of Mn into the CdS lattices. As excited by 3.815 eV, the Mn^{2+} emission at around 2.15 eV, originating from the d−d ($^4T_1 \rightarrow {}^6A_1$) transition, is greatly enhanced at temperatures below 50−80 K. The time-resolved PL spectrum reveals that the decay time of Mn^{2+} emission is 1, 0.7, and 0.55 ms, respectively, for the Mn content $x = 0.1$, 0.2, and 0.3. The Mn doping reduces significantly the decay time of band-edge emission from 590 ps to 20−30 ps. The magneto-PL measurement under a magnetic field shows significant suppression of Mn^{2+} emission and enhancement of DAP emission, suggesting that the excitation of Mn^{2+} involves energy transfer from the band excitons. From the peak position of DAP emission, we estimate that the band gap can increase by ~100 meV as the Mn content increases from $x = 0.1$ to 0.3. Finally, we suggest that the Mn doping of CdS NWs has a great deal of potential for applications in magnetooptical nanodevices.

Acknowledgment. This work is supported by KRF (R14-2003-033-01003-0; R02-2004-000-10025-0; 2003-015-C00265), KIST (2E18740-05-062), and National Creative Research Initiative of KOSEF. The SEM, field-emission TEM, HVEM, and SQUID measurements were performed at the Korea Basic Science Institute. Experiments at PLS were supported in part by MOST and POSTECH.

References and Notes

(1) (a) Ohno, H. *Science* **1998**, *281*, 951. (b) Ohno, Y.; Young, D. K.; Beschoten, B.; Matsukura, F.; Ohno, H.; Awschalom, D. D. *Nature* (*London, U.K.*) **1999**, *402*, 790. (c) Ohno, H.; Chiba, D.; Matsukura, F.; Omiya, T.; Abe, E.; Dietl, T.; Ohno, Y.; Ohtani, K. *Nature* (*London, U.K.*) **2000**, *408*, 944.

(2) Fiederling, R.; Keim, M.; Reuscher, G.; Ossau, W.; Schmidt, G..; Waag, A.; Molenkamp, L. W. *Nature* (*London, U.K.*) **1999**, *402*, 787.

(3) Dietl, T.; Ohno, H.; Matsukura, F.; Cibert, J.; Ferrand, D. *Science* **2000**, *287*, 1019.

(4) Wolf, S. A.; Awschalom, D. D.; Buhrman, R. A.; Daughton, J. M.; von Molnár, S.; Roukes, M. L.; Chtchelkanova, A. Y.; Treger, D. M. *Science* **2001**, *294*, 1488.

(5) (a) Chamarro, M. A.; Voliotis, V.; Grousson, R.; Lavallard, P.; Gacoin, T.; Counio, G.; Boilot, J. P.; Cases, R. *J. Cryst. Growth* **1996**, *159*, 853. (b) Counio, G.; Gacoin, T.; Boilot, J. P. *J. Phys. Chem. B* **1998**, *102*, 5257.

(6) (a) Levy, L.; Feltin, N.; Ingert, D.; Pileni, M. P. *J. Phys. Chem. B* **1997**, *101*, 9153. (b) Levy, L.; Ingert, D.; Feltin, N.; Pileni, M. P. *Adv. Mater.* **1998**, *10*, 53. (c) Feltin, N.; Levy, L.; Ingert, D.; Pileni, M. P. *J. Phys. Chem.* B **1999**, *103*, 4.

(7) Liu, S.-M.; Liu, F.-Q.; Guo, H.-Q.; Zhang, Z.-H.; Wang, Z.-G. *Solid State Commun.* **2000**, *115*, 615.

(8) Guo, S.; Konopny, L.; Popovitz-Biro, R.; Cohen, H.; Sirota, M.; Lifshitz, E.; Lahav, M. *Adv. Mater.* **2000**, *12*, 302.

(9) Jun, Y.; Jung, Y.; Cheon, J. *J. Am. Chem. Soc.* **2002**, *124*, 615.

(10) Kanemitsu, Y.; Matsubara, H.; White, C. W. *Appl. Phys. Lett.* **2002**, *81*, 535.

(11) Bol, A. A.; van Beek, R.; Ferwerda, J.; Meijerink, A. *J. Phys. Chem. Solids* **2003**, *64*, 247.

(12) Barglik-Chory, C.; Remenyi, C.; Dem, C.; Schmitt, M.; Kiefer, W.; Gould, C.; Rüster, C.; Schmidt, G.; Hofmann, D. M.; Pfisterer, D.; Müller, G. *Phys. Chem. Chem. Phys.* **2003**, *5*, 1639.

(13) (a) Yang, H.; Holloway, P. H. *Appl. Phys. Lett.* **2003**, *82*, 1965. (b) Yang, H.; Holloway, P. H.; Santra, S. *J. Chem. Phys.* **2004**, *121*, 7421. (c) Santra, S.; Yang, H.; Holloway, P. H.; Stanley, J. T.; Mericle, R. A. *J. Am. Chem. Soc.* **2005**, *127*, 1656.

(14) Pang, Q.; Guo, B. C.; Yang, C. L.; Yang, S. H.; Gong, M. L.; Ge, W. K.; Wang, J. N. *J. Cryst. Growth* **2004**, *269*, 213.

(15) (a) Kouzema, A. V.; Fröba, M.; Chen, L.; Klar, P. J.; Heimbrodt, W. *Adv. Funct. Mater.* **2005**, *15*, 168. (b) Brieler, F. J.; Grundmann, P.; Fröba, M.; Chen, L.; Klar, P. J.; Heimbrodt, W.; von Nidda, H.-A. K.; Kurz, T.; Loidl, A. *Chem. Mater.* **2005**, *17*, 795. (c) Brieler, F. J.; Fröba, M.; Chen, L.; Klar, P. J.; Heimbrodt, W.; von Nidda, H.-A. K.; Loidl, A. *Chem. Eur. J.* **2005**, *8*, 185. (d) Brieler, F. J.; Grundmann, P.; Fröba, M.; Chen, L.; Klar, P. J.; Heimbrodt, W.; von Nidda, H.-A. K.; Kurz, T.; Loidl, A. *Eur. J. Inorg. Chem.* **2005**, 3597.

(16) (a) Han, D. S.; Park, J.; Rhie, K. W.; Chang, J. *Appl. Phys. Lett.* **2005**, *86*, 032506. (b) Choi, H.-J.; Seong, H.-K.; Chang, J.; Lee, K.-I.; Park, Y.-J.; Kim, J.-J.; Lee, S.-K.; He, R.; Kuykendall, T.; Yang, P. *Adv. Mater.* **2005**, *17*, 1351. (c) Han, D. S.; Bae, S. Y.; Seo, H. W.; Kang, Y. J.; Park, J.; Lee, G.; Ahn, J.-P.; Kim, S.; Chang, J. *J. Phys. Chem. B* **2005**, *109*, 9311. (d) Krusin-Elbaum, L.; Newns, D. M.; Zeng, H.; Derycke, V.; Sun, J. Z.; Sandstrom, R. *Nature* **2004**, *431*, 672.

(17) (a) Wang, Q. S.; Xu, Z. D.; Nie, Q. L.; Yue, L. H.; Chen, W. X.; Zheng, Y. F. *Solid State Commun.* **2004**, *130*, 607. (b) Wang, Q.; Xu, Z.; Yue, L.; Chen, W. *Opt. Mater.* **2004**, *27*, 453.

(18) Radovanoic, P. V.; Barrelet, C. J.; Gradeèak, S.; Qian, F.; Lieber, C. M. *Nano Lett.* **2005**, *5*, 1407.

(19) Rodic, D.; Spasojevic, V.; Bajorek, A.; Onnerud, P. *J. Magn. Magn. Mater.* **1996**, *152*, 159.

(20) Thomas, D. G.; Hopfield, J. J. *Phys. Rev.* **1962**, *128*, 2135.

(21) Enrlich, Ch.; Busse, W.; Gumlich, H.-E.; Tschierse, D. *J. Cryst. Growth* **1985**, *72*, 371.
(22) Goede; O.; Thong, D. D. *Phys. Status Solidi B* **1984**, *124*, 343.
(23) (a) Spanhel, L.; Hasse, M.; Weller, H.; Henglein, *J. Am. Chem. Soc.* **1987**, *109*, 5649. (b) Spanhel, L.; Anderson, M. A. *J. Am. Chem. Soc.* **1990**, *112*, 2, 2278.
(24) Kamat, P. V.; Dimitrijevic, N. M.; Nozik, A. J. *J. Phys. Chem. Soc.* **1989** *93*, 2873.
(25) Suh, J. S.; Lee, S. *Chem. Phys. Lett.* **1997**, *281*, 384.
(26) Henry, C. H.; Faulkners, R. A.; Nassau, K. *Phys. Rev.* **1969**, *183*, 798.
(27) Nawrocki, M.; Rubo, Yu. G.; Lascaray, J. P.; Coquillat, D. *Phys. Rev. B* **1995**, *52*, R2241.
(28) Tsai, C. T.; Chen, S. H.; Chuu, D. S.; Chou, W. C. *Phys. Rev. B* **1996**, *54*, 11555.
(29) Ikeda, M.; Itoh, K.; Sato, H. *J. Phys. Soc. Jpn.* **1968**, *25*, 455.
(30) Khoi, N. T.; Ginter, J.; Twardowski, *Phys. Status Solidi B* **1983**, *117*, 67.